A Highly Flexible Trajectory Model Based on the Primitives of Brownian Fields—Part II: Analysis of the Statistical Properties

Alireza Borhani and Matthias Pätzold
Faculty of Engineering and Science, University of Agder
P.O. Box 509, 4898 Grimstad, Norway
Emails: {alireza.borhani, matthias.paetzold}@uia.no

***Abstract*—In the first part of our paper, we have proposed a highly flexible trajectory model based on the primitives of Brownian fields (BFs). In this second part, we study the statistical properties of that trajectory model in depth. These properties include the autocorrelation function (ACF), mean, and the variance of the path along each axis. We also derive the distribution of the angle-of-motion (AOM) process, the incremental travelling length process, and the overall travelling length. It is shown that the path process is in general non-stationary. We show that the AOM and the incremental travelling length processes can be modelled by the phase and the envelope of a complex Gaussian process with nonidentical means and variances of the quadrature components. In accordance with empirical studies, we proof that the AOM process does not follow the uniform distribution. As special cases, we show that the incremental travelling length process follows the Rice and Nakagami-q distributions, whereas the overall travelling path can be modelled by a random variable following either the Gaussian or the lognormal distribution. The flexibility of the results is demonstrated and discussed extensively. It is shown that the results are in line with those of real-world user tracings. The results can be used in many areas of wireless communications.**

***Index Terms* — Trajectory model, mobility model, Brownian fields, autocorrelation function, angle-of-motion, travelling length.**

I. INTRODUCTION

To evaluate the usefulness of mobility models for system-level analysis, their statistical properties need to be studied thoroughly. Many spatial features of the models listed, e.g., in [1]–[3] are revealed by investigating their statistical characteristics. However, a gap in the related literature is that there exist very limited solid mathematical studies on the statistical properties of spatial trajectory models. These models have often been proposed in form of Java-based simulation models from which obtaining a sound understanding of the statistical characteristics is not an easy task. The path processes' mean, variance, ACF, AOM, and the travelling length are among the most important spatial characteristics that play important roles in the performance analysis of the overall system. These quantities can also be very useful for the parametrization of the mobility model itself.

The random walk [4], [5], random waypoint [6], Gauss-Markov [7], city section [8], and the pursue [9] mobility models are examples of established mobility models, in which the physical location (trajectory) of the user is often determined by mapping given distributions of the speed/travelled distance and the AOM on the Euclidian space. Despite the temporal properties of these models, their spatial characteristics have rarely been studied. The spatial node distribution of the random waypoint mobility model (as a temporal model) has been investigated, e.g., in [10]–[12]. The expected epoch time and the number of states visited at a fixed time are two important temporal properties of a mobility model that have often been investigated [13]. Given a typical mobility model, the effect of the speed distribution on computer-based simulations was also studied in [15]. Different from the aforementioned temporal mobility models, a fully spatial trajectory model, to which different temporal features (speed scenarios) can be applied, was proposed in the first part [16] of our paper. The superiorities of a spatial trajectory model over the temporal one have been addressed in [16] (see Section I).

In this second part of our paper, we analyze the statistical properties of the trajectory model in [16], which belongs to the class of spatial trajectory models that are based on the primitives of BFs. The random components of the path model are derived from Gaussian processes, which are defined in position rather than time. Therefore, our analysis is fundamentally different from those in [10]–[12], where the distribution of nodes associated with a temporal mobility model was pursued. Herein, we derive the spatial mean and variance of the stochastic spatial trajectory model. A closed-form expression for the ACF of the path process is also provided. Moreover, we introduce a complex spatial increment process, from which the AOM and the incremental travelling length processes are derived. The first-order density of these processes is presented in closed form. By summing up the incremental travelling lengths, we compute the overall travelling length and its probability density function (PDF). The results are illustrated and discussed in detail.

We proof that the path process is in general non-stationary. Furthermore, it is shown that the AOM and the incremental travelling length processes are modelled by the phase and the envelope of a complex Gaussian process with nonidentical means and variances of the quadrature components. We show that the AOM and the incremental travelling length are in general non-stationary processes. In this connection, we demonstrate that the AOM process does not follow the uniform distribution, which agrees with empirical traces reported in [17]. However, the uniform AOM can be obtained as a special case. In addition, we proof that the incremental travelling length process follows the Rice and Nakagami-q

distributions as special cases. For the path based on the primitives of the standard BFs, we show that the overall travelling length follows closely the lognormal distribution, which is in line with many real-world tracing records [17]–[20]. For the path based on the standard BF, we proof that the overall travelling length follows the Gaussian distribution, which has been reported from studies in dense urban environments [21]–[27].

The statistical properties provided in this second paper are very useful in many areas of science, such as wireless communications and vehicular technologies. The results of this paper can be used by researchers dealing with ad hoc networks, localization (positioning), network mobility protocols, and mobile radio channel modelling under non-stationary conditions[1].

The remainder of this paper is organized as follows. Section II recalls the principles of the trajectory model proposed in the first part of our paper. The statistical properties of the model are investigated in Section III. Section IV studies the spatial characteristics of the proposed model. To provide a sound understanding of the results, two important special cases of the path model are discussed in Section V. The numerical results are presented in Section VI. Eventually, the conclusion is presented in Section VII.

II. A Brief Review of the Trajectory Model

With reference to the first part [16] of our paper, we model a path starting from (x_s, y_s) and terminating at or in the proximity of a given destination point (x_d, y_d) by the trajectory ${}_p\mathcal{T}$ designed by the following pair

$$ {}_p\mathcal{T}: \left\{ ({}_px(l), {}_py(l)) \;\middle|\; \begin{array}{l} {}_px(l) = x_s + k_d\, l\delta_x + \sigma_x\, {}_pW_x(l, k_b) \\ {}_py(l) = y_s + k_d\, l\delta_y + \sigma_y\, {}_pW_y(l, k_b) \end{array} \right\} \tag{1} $$

in which the position variable $l \in [0, L]$ is the countable parameter of the standard BF in a 2D spatial sample space (see Section III-B of Part I). For a positive integer L, the terms $\delta_x = (x_d - x_s)/L$ and $\delta_y = (y_d - y_s)/L$ denote the deterministic increments along each axis. The drift parameter k_d acts as a switch to control the presence of such a deterministic drift that forces the path to evolve towards the destination point (x_d, y_d) (see Section IV-C of Part I). The parameter σ_x (σ_y) is to control the randomness of the path ${}_px(l)$ (${}_py(l)$) along the x-axis (y-axis)[2] (see Section IV-A of Part I). Furthermore, the objective of the partial random bridge, defined as

$$ {}_pW_x(l, k_b) = {}_pB_x(l) - \frac{k_b\, l}{L}\, {}_pB_x(L) \tag{2} $$

is to model the randomness of the path along each axis by means of the pth primitive ${}_pB_x(l)$ of the standard BF $B_x(l)$ associated with the x-axis. It is assumed that the processes ${}_pB_x(l)$ and ${}_pB_y(l)$ are mutually independent. The parameter k_b is called the bridge parameter, which determines the integration degree of the bridge to the destination point (see Section IV-B of Part I). In addition, the primitive p determines the smoothness level of the path. We remind that the level of smoothness increases by increasing p (see Section IV-D of Part I).

The trajectory ${}_p\mathcal{T}$ in (1) has been designed in such a way that allows 1) arriving at a predefined destination point (x_d, y_d) if the bridge is fully established, i.e., $k_b = 1$, 2) arriving at a target zone with a predefined radius and centre (see Theorem 1 and Corollary 1 of Part I) if the bridge is partially established, i.e., $0 < k_b < 1$, 3) a totally random point in the two-dimensional (2D) plane if the bridge is broken, i.e., $k_b = 0$, and finally 4) bridging back (closed loop) to the starting point (x_s, y_s) if the bridge is fully established, i.e., $k_b = 1$, but the drift component does not exist, i.e., $k_d = 0$. The entire configurations above plus several others have been shown and extensively discussed in Part I of our paper. In addition, the speed adaptivity of the proposed trajectory model has been explained in Part I (see Section IV-D in [16]).

III. Statistical Properties of the Process ${}_px(l)$ (${}_py(l)$)

In this section, we investigate the statistical properties of the process ${}_px(l)$ ($l = 1, 2, ..., L$). We first derive the first-order density[3] of ${}_px(l)$ and then study the corresponding mean, ACF, and variance. Owing to the statistical equivalence of the path ${}_p\mathcal{T}$ along the x- and y-axis (see (1)), the statistical characteristics of the process ${}_py(l)$ can be obtained from those of ${}_px(l)$ by replacing x by y in the respective equations.

A. First-Order Density of ${}_px(l)$

The process ${}_px(l)$ in (1) is a shifted version of the bridge process ${}_pW_x(l, k_b)$, which is consist of the pth primitive of the standard BF $B_x(l)$, given by

$$ {}_pB_x(l) = \int_0^l {}_{p-1}B_x(l')\, dl' \quad \forall p = 1, 2, \ldots . \tag{3} $$

With reference to Part I of the series of two papers, the process ${}_pB_x(l)$ in (3) is a Gaussian process of the form $N(0, \sigma^2_{{}_pB}(l))$, where [31]

$$ \sigma^2_{{}_pB_x}(l) = \frac{l^{2p+1}}{(p!)^2(2p+1)}. \tag{4} $$

Referring to (2), the bridge process ${}_pW_x(l, k_b)$ is a linear combination of two Gaussian processes. This allows us to conclude that the first-order density of ${}_px(l)$ in (1) is a normal distribution of the form $N(m_{{}_px}(l), \sigma^2_{{}_px}(l))$, where the mean $m_{{}_px}(l)$ and the variance $\sigma^2_{{}_px}(l)$ are derived in Sections III-B and III-D, respectively.

It is also worth mentioning that the autocovariance function $r^c_{{}_pB_x\, {}_pB_x}(l_i, l_j)$ of ${}_pB_x(l)$ is given by the following expression [32]

$$ r^c_{{}_pB_x\, {}_pB_x}(l_i, l_j) = \frac{1}{(p!)^2} \int_0^{\min(l_i, l_j)} (l_i - l')^p (l_j - l')^p\, dl'. \tag{5} $$

[1]For the application in channel modelling, see [28] and [29].

[2]Due to the symmetry of the trajectory model, the statistical properties of ${}_px(l)$ and ${}_py(l)$ are the same. Therefore, and for fluency reasons, we henceforth avoid repeating the analogy between the essential properties of the path along the x- and y-axis.

[3]According to [30, p. 375], the fist-order density of a process is nothing else than its time-varying PDF in the context of stochastic processes.

The variance $\sigma^2_{{}_pB_x}(l)$ and the autocovariance function $r^c_{{}_pB_x\,{}_pB_x}(l_i,l_j)$ of ${}_pB_x(l)$ play key roles in the analysis of the statistical properties of the trajectory ${}_p\mathcal{T}$ in (1).

B. Mean of ${}_px(l)$

The mean $m_{{}_px}(l)$ of the process ${}_px(l)$ in (1) can be computed as follows

$$\begin{aligned} m_{{}_px}(l) &= E\{x_s + k_d l\delta_x + \sigma_{xp} W_x(l,k_b)\} \\ &= x_s + k_d l\delta_x + \sigma_x E\left\{{}_pB_x(l) - \frac{k_b l}{L}{}_pB_x(L)\right\} \\ &= x_s + k_d l\delta_x + \sigma_x E\{{}_pB_x(l)\} - \frac{k_b l}{L}E\{{}_pB_x(L)\} \\ &= x_s + k_d l\delta_x \end{aligned} \quad (6)$$

where we have used $E\{{}_pB_x(l)\} = 0$ for $l = 0, 1, ..., L$. For $k_d = 1$ and $\delta_x > 0$, the mean $m_{{}_px}(l)$ in (6) increases linearly with the position index l, which means that the process ${}_px(l)$ is neither strict-sense stationary nor wide-sense stationary. This can be attributed to the drift of the path, which establishes the dependency of the mean $m_{{}_px}(l)$ upon the position index l. If the drift does not exist, i.e., $k_d = 0$, then the mean $m_{{}_px}(l)$ equals the starting length x_s.

C. Autocorrelation Function of ${}_px(l)$

The expectation $E\{{}_px(l_i)\,{}_px(l_j)\}$ equals the ACF $r_{{}_px\,{}_px}(l_i,l_j)$ of the process ${}_px(l)$ at the position indices l_i and l_j. It can be shown (see Appendix A) that

$$\begin{aligned} r_{{}_px\,{}_px}(l_i,l_j) &= m_{{}_px}(l_i)m_{{}_px}(l_j) + \sigma_x^2\left(r^c_{{}_pB_x\,{}_pB_x}(l_i,l_j)\right. \\ &- \frac{k_b l_j}{L} r^c_{{}_pB_x\,{}_pB_x}(l_i,L) - \frac{k_b l_i}{L} r^c_{{}_pB_x\,{}_pB_x}(L,l_j) \\ &+ \left.\frac{k_b^2 l_i l_j}{L^2} r^c_{{}_pB_x\,{}_pB_x}(L,L)\right) \end{aligned} \quad (7)$$

where the autocovariance function $r^c_{{}_pB_x\,{}_pB_x}(l_i,l_j)$ is given by[4] (5). The ACF $r_{{}_px\,{}_px}(l_i,l_j)$ in (7) cannot be written as a function of the difference $l_d = l_i - l_j$, which confirms that ${}_px(l)$ is not wide-sense stationary.

An important special case occurs if we set one of the arguments of the ACF in (7) to 0. In this case, (7) reduces to the following expression

$$\begin{aligned} r_{{}_px\,{}_px}(0,l_j) &= m_{{}_px}(0)m_{{}_px}(l_j) + \sigma_x^2\left(r^c_{{}_pB_x\,{}_pB_x}(0,l_j)\right. \\ &- \left.\frac{k_b l_j}{L} r^c_{{}_pB_x\,{}_pB_x}(0,L)\right) \\ &= m_{{}_px}(0)m_{{}_px}(l_j) \\ &= x_s(x_s + k_d l_j\delta_x) \end{aligned} \quad (8)$$

where we have used $r^c_{{}_pB_x\,{}_pB_x}(0,l_j) = r^c_{{}_pB_x\,{}_pB_x}(0,L) = 0$. The recent reduction originates from the fact that $\min(0, l_j) = 0$ in (5) forces $r^c_{{}_pB_x\,{}_pB_x}(0,l_j)$ to 0. With the same token, it can be shown that $r_{{}_py\,{}_py}(0,l_j) = m_{{}_py}(0)m_{{}_py}(l_j)$, from which it can be concluded that the correlation between the starting point and any heading point is determined by the product of the corresponding mean values. If one of the mean values is zero, no correlation exists. It can also be shown that if the bridge is fully established, i.e., $k_b = 1$, then $r_{{}_px\,{}_px}(L,l_j) = r_{{}_px\,{}_px}(l_j,L) = m_{{}_px}(L)m_{{}_px}(l_j)$. In this case, the correlation between the terminating point and its posterior points is also determined by the product of the corresponding mean values.

[4]To cope with the discreteness of the position index l, one may simply use the equivalent Riemann sum of the integral in (5).

D. Variance of ${}_px(l)$

The variance $\sigma^2_{{}_px}(l)$ of the process ${}_px(l)$ is computed as follows

$$\begin{aligned} \sigma^2_{{}_px}(l) &= r_{{}_px\,{}_px}(l,l) - m^2_{{}_px}(l) \\ &= \sigma_x^2\left(r^c_{{}_pB_x\,{}_pB_x}(l,l) - 2\frac{k_b l}{L} r^c_{{}_pB_x\,{}_pB_x}(l,L)\right. \\ &+ \left.\frac{k_b^2 l^2}{L^2} r^c_{{}_pB_x\,{}_pB_x}(L,L)\right). \end{aligned} \quad (9)$$

It can be shown that the variance $\sigma^2_{{}_px}(l)$ of the process ${}_px(l)$ in (9) is a monotonically increasing function in p. This is intuitively due to the fact that the integration over the standard BF increases the correlation between the random components. Furthermore, it can be verified that $\lim_{l\to 0}\sigma^2_{{}_px}(l) = 0$. Analogously, one can write $\lim_{l\to 0}\sigma^2_{{}_py}(l) = 0$. The two recent limits state that the randomness of the points near the starting point $({}_px(0), {}_py(0))$ (or equivalently (x_s, y_s)) tends to zero. The randomness of the terminating point $({}_px(L), {}_py(L))$ and the points in its close vicinity, however, do not vanish, as the limit

$$\begin{aligned} \lim_{l\to L}\sigma^2_{{}_px}(l) &= \sigma_x^2(1-k_b)^2 r^c_{{}_pB_x\,{}_pB_x}(L,L) \\ &= \sigma_x^2(1-k_b)^2\sigma^2_{{}_pB_x}(L) \end{aligned} \quad (10)$$

is in general not equal to 0. If $k_b \to 1$, then $\lim_{l\to L}\sigma^2_{{}_px}(l) = 0$. It is also worth mentioning that the result in (10) is equal to the parameter $\sigma^2_{D_d}$ of the Rayleigh distributed distance D_d between the terminating point $({}_px(L), {}_py(L))$ and the destination point (x_d, y_d), which opens an alternative way to proof Theorem 1 of Part I [16]. We also remark that the variance $\sigma^2_{{}_px}(l)$ of the process ${}_px(l)$ is very useful for adjusting the standard deviation σ_x as one of the important model parameters (see Section V-B in [16]).

IV. Spatial Characteristic of the Trajectory ${}_p\mathcal{T}$

This section deals with the spatial processes, which consist of the elements ${}_px(l)$ and ${}_py(l)$ of the trajectory ${}_p\mathcal{T}$ along the x- and y-axis.

A. Spatial Increment Process

Let the complex process ${}_ps(l) = {}_ps_x(l) + j\,{}_ps_y(l)$ ($l = 1, 2, ..., L$) define the spatial increment process of the trajectory ${}_p\mathcal{T}$, where ${}_ps_x(l) = {}_px(l) - {}_px(l-1)$ and ${}_ps_y(l) = {}_py(l) - {}_py(l-1)$ are the increments along the x- and y-axis, respectively, and $j = \sqrt{-1}$.

Theorem 1. *The spatial increment ${}_ps(l)$ follows the complex Gaussian distribution of the form $CN(\boldsymbol{m}_{{}_ps}, \boldsymbol{C}_{{}_ps})$, where $\boldsymbol{m}_{{}_ps} = [k_d\delta_x,\ k_d\delta_y]^T$,*

$$\boldsymbol{C}_{{}_{p}s} = \begin{pmatrix} \sigma^2_{{}_{p}s_x}(l) & 0 \\ 0 & \sigma^2_{{}_{p}s_y}(l) \end{pmatrix} \tag{11}$$

$$\begin{aligned}\sigma^2_{{}_{p}s_x}(l) = \sigma^2_x \Big(& r^c_{{}_{p}B_x\,{}_{p}B_x}(l,l) + r^c_{{}_{p}B_x\,{}_{p}B_x}(l-1,l-1) \\ & + \frac{k_b^2}{L^2} r^c_{{}_{p}B_x\,{}_{p}B_x}(L,L) - 2r^c_{{}_{p}B_x\,{}_{p}B_x}(l,l-1) \\ & - \frac{2k_b}{L} r^c_{{}_{p}B_x\,{}_{p}B_x}(l,L) + \frac{2k_b}{L} r^c_{{}_{p}B_x\,{}_{p}B_x}(l-1,L) \Big)\end{aligned} \tag{12}$$

and $\sigma^2_{{}_{p}s_y}(l)$ can be obtained from (12) by replacing the superscript x by y.

Proof: See Appendix B. ■

From Theorem 1, it can be concluded that the spatial increment process ${}_{p}s(l)$ is not strict-sense stationary, as its first-order density $CN\left(\boldsymbol{m}_{{}_{p}s}, \boldsymbol{C}_{{}_{p}s}\right)$ varies in l. The spatial increment process ${}_{p}s(l)$ is very useful for deriving the AOM process and the incremental travelling length process of the path ${}_{p}\mathcal{T}$, as will be shown in the next two subsections.

B. AOM Process

The AOM ${}_{p}\alpha^v(l)$ process, defined as

$$\begin{aligned} {}_{p}\alpha^v(l) &= \arctan\left(\frac{{}_{p}y(l) - {}_{p}y(l-1)}{{}_{p}x(l) - {}_{p}x(l-1)}\right) \\ &= \arctan\left(\frac{{}_{p}s_y(l)}{{}_{p}s_x(l)}\right) \end{aligned} \tag{13}$$

can be considered as the phase of the spatial increment process ${}_{p}s(l)$.

Corollary 1. *The first-order density $p_{{}_{p}\alpha^v}(\alpha^v; l)$ of the AOM process ${}_{p}\alpha^v(l)$ in (13) is given by the following expression*

$$\begin{aligned} p_{{}_{p}\alpha^v}(\alpha^v; l) &= \frac{1}{4\pi g_1(\alpha^v; l)\sigma_{{}_{p}s_x}(l)\sigma_{{}_{p}s_y}(l)} \\ &\times \quad exp\left\{-\frac{1}{2}\left(\frac{k_d^2\delta_x^2}{\sigma^2_{{}_{p}s_x}(l)} + \frac{k_d^2\delta_y^2}{\sigma^2_{{}_{p}s_y}(l)}\right)\right\} \\ &\times \left(1 + \frac{\sqrt{\pi} g_2(\alpha^v; l)}{2\sqrt{g_1(\alpha^v; l)}}\, erfc\left(\frac{-g_2(\alpha^v; l)}{2\sqrt{g_1(\alpha^v; l)}}\right)\right. \\ &\times \quad \left. exp\left\{\frac{g_2^2(\alpha^v; l)}{4g_1(\alpha^v; l)}\right\}\right) \end{aligned} \tag{14}$$

where

$$g_1(\alpha^v; l) = \frac{1}{2}\left(\frac{\cos^2(\alpha^v)}{\sigma^2_{{}_{p}s_x}(l)} + \frac{\sin^2(\alpha^v)}{\sigma^2_{{}_{p}s_y}(l)}\right) \tag{15}$$

$$g_2(\alpha^v; l) = k_d\left(\frac{\delta_x \cos(\alpha^v)}{\sigma^2_{{}_{p}s_x}(l)} + \frac{\delta_y \sin(\alpha^v)}{\sigma^2_{{}_{p}s_x}(l)}\right) \tag{16}$$

and erfc$(\cdot)$ stands for the complementary error function [33, p. 887].

Proof: With reference to Theorem 1, the spatial increment ${}_{p}s(l)$ follows the complex Gaussian distribution of the form $CN\left(\boldsymbol{m}_{{}_{p}s}, \boldsymbol{C}_{{}_{p}s}\right)$. The phase and the envelope of complex Gaussian processes with correlated quadratures and non-identical means (variances) have been studied in [34] and [35]. Herein, the correlation ρ between the inphase and quadrature components of the spatial increment process ${}_{p}s(l)$ is zero, i.e., $\rho = C_{12} = C_{21} = 0$. Starting from the phase distribution of a complex Gaussian distribution with uncorrelated quadratures in [35, Eq. (2)], setting $\rho = 0$, and performing some straightforward mathematical manipulations results in (14). ■

In accordance with the spatial increment process ${}_{p}s(l)$, the AOM process ${}_{p}\alpha^v(l)$ in (13) is not first-order stationary, as its first-order density $p_{{}_{p}\alpha^v}(\alpha^v; l)$ in (14) depends on position index l. The special case of $p = 0$, however, results in a stationary AOM process ${}_{p}\alpha^v(l)$. In this case, it is straightforward to show by means of (5) that the variance $\sigma^2_{{}_{p}s_x}(l)$ in (12) reduces to

$$\sigma^2_{{}_{0}s_x} = \sigma^2_x\left(1 + \frac{k_b^2}{L} - 2\frac{k_b}{L}\right) \tag{17}$$

which does not change in l, stopping the variations of $p_{{}_{p}\alpha^v}(\alpha^v; l)$ in l as well (see (14)–(16)). Another stationary case occurs if we decrease the variances σ_x^2 and σ_y^2 towards zero. In this case, $p_{{}_{p}\alpha^v_l}(\alpha^v; l)$ in (14) tends to the delta function located at $\alpha^v = \arctan(\delta_y/\delta_x)$, which is independent of l. Notice that $\arctan(\delta_y/\delta_x)$ indicates the general drift of the path ${}_{p}\mathcal{T}$ in (1).

An important property of the AOM ${}_{p}\alpha^v(l)$ of the proposed trajectory model is that ${}_{p}\alpha^v(l)$ is in general not uniformly distributed. The non-uniform distribution of the AOM has also been reported from the real-world tracing in [17]. Nonetheless, under special conditions, the first-order density $p_{{}_{p}\alpha^v}(\alpha^v; l)$ in (14) can be simplified to a constant value, indicating that the AOM ${}_{p}\alpha^v(l)$ is uniformly distributed. Notice that the uniform distribution of the AOM is one of the widely made assumptions in the synthetic mobility models proposed in the literature, which is, however, not necessarily true.

C. Incremental Travelling Length Process

The incremental travelling length process ${}_{p}d(l)$ is defined by the following expression

$$\begin{aligned} {}_{p}d(l) &= \sqrt{\left({}_{p}x(l) - {}_{p}x(l-1)\right)^2 + \left({}_{p}y(l) - {}_{p}y(l-1)\right)^2} \\ &= \sqrt{{}_{p}s_x^2(l) + {}_{p}s_y^2(l)} \end{aligned} \tag{18}$$

which is the envelope of the spatial increment process ${}_{p}s(l)$.

Corollary 2. *The first-order density $p_{{}_{p}d}(d; l)$ of the incremen-*

tal travelling length process ${}_pd(l)$ equals

$$p_{{}_pd}(d;l) = \frac{d}{\sigma_{{}_ps_x}(l)\sigma_{{}_ps_y}(l)} exp\left\{-\frac{\sigma^2_{{}_ps_x}(l)+\sigma^2_{{}_ps_y}(l)}{4\sigma^2_{{}_ps_x}(l)\sigma^2_{{}_ps_y}(l)}d^2 - \frac{k_d^2\left(\delta_x^2\sigma^2_{{}_ps_y}(l)+\delta_y^2\sigma^2_{{}_ps_x}(l)\right)}{2\sigma^2_{{}_ps_x}(l)\sigma^2_{{}_ps_y}(l)}\right\}\sum_{n=0}^{\infty}\varepsilon_n \times \cos\left(ng_3(l)\right) I_n\left(\frac{\sigma^2_{{}_ps_x}(l)-\sigma^2_{{}_ps_y}(l)}{4\sigma^2_{{}_ps_x}(l)\sigma^2_{{}_ps_y}(l)}d^2\right) \times I_{2n}\left(\frac{k_d\sqrt{\delta_x^2\sigma^4_{{}_ps_y}(l)+\delta_y^2\sigma^4_{{}_ps_x}(l)}}{\sigma^2_{{}_ps_x}(l)\sigma^2_{{}_ps_y}(l)}d\right) \tag{19}$$

where

$$g_3(l) = 2\arccos\left(\frac{\delta_x\sigma^2_{{}_ps_y}(l)}{\sqrt{\delta_x^2\sigma^4_{{}_ps_y}(l)+\delta_y^2\sigma^4_{{}_ps_x}(l)}}\right) \tag{20}$$

and $I_n(\cdot)$ denotes the nth order modified Bessel function of the first kind [33, p. 629]. The parameter ε_n stands for the Neumann factor [36], which equals 1 for $n = 0$, and 2 for $n = 1, 2, ...$

Proof: Following the discussion provided in the proof of Corollary 1, setting $\rho = 0$ in the envelope distribution in [35, Eq. (1)], and applying simple mathematical manipulations give the PDF in (19). ∎

It has been shown in [35] that the infinite series in (19) is convergent. It is also not difficult to verify that $\forall p, \lim_{d\to\infty} p_{{}_pd(l)}(d;l) \to 0$. This means that the probability of *jumping far* from $({}_px(l-1), {}_py(l-1))$ to $({}_px(l), {}_py(l))$ tends to zero for all $p = 0, 1, ...$, which is a prerequisite for a realistic path model. An important property of the PDF $p_{{}_pd}(d;l)$ in (19) is its dependency on l, which allows us to conclude that the incremental travelling length process ${}_pd(l)$ in (18) is in general non-stationary in the strict sense. Analogously to the discussion in Section IV-B, this dependency can be relaxed by setting $p = 0$. In this case, $\sigma^2_{{}_ps_x}(l)$ is given by (17), which makes $p_{{}_pd}(d;l)$ in (19) independent of l.

Another important special case is attained if $\sigma_x = \sigma_y = \sigma_0$ and $\delta_x = \delta_y = \delta_0$. In this case, the PDF $p_{{}_pd}(d;l)$ in (19) reduces to the Rice distribution of the following form

$$p_{{}_pd}(d;l) = \frac{d}{\sigma^2_{{}_ps_x}(l)}\exp\left\{-\frac{2k_d^2\delta_0^2+d^2}{2\sigma^2_{{}_ps_x}(l)}\right\} I_0\left(\frac{k_d\delta_0\sqrt{2}}{\sigma^2_{{}_ps_x}(l)}d\right). \tag{21}$$

It is worth mentioning that the Rice distribution above is not a function of l if $p = 0$. Given this special case, the mean $m_{{}_0d}$ and the variance $\sigma^2_{{}_0d}$ of the Rician distributed incremental travelling length ${}_0d(l)$ is obtained by (see, e.g., [37, p. 28])

$$m_{{}_0d} = \sigma^2_{{}_0s_x}\sqrt{\frac{\pi}{2}}\,{}_1F_1\left(-\frac{1}{2};\,1;\,-\frac{k_d^2\delta_0^2}{\sigma^2_{{}_0s_x}}\right) \tag{22}$$

and

$$\sigma^2_{{}_0d} = 2\sigma^2_{{}_0s_x} + 2k_d^2\delta_0^2 - m^2_{{}_0d} \tag{23}$$

respectively, where the function ${}_pF_q(a_1, ..., a_p; b_1, ..., b_q; x)$ stands for the generalized hypergeometric function [33, p. 1010].

If the drift component does not exist, i.e., $k_d = 0$, the PDF $p_{{}_pd}(d;l)$ in (19) is simplified to the Nakagami-q distribution of the form

$$p_{{}_pd}(d;l) = \frac{d}{\sigma_{{}_ps_x}(l)\sigma_{{}_ps_y}(l)}\exp\left\{-\frac{\sigma^2_{{}_ps_x}(l)+\sigma^2_{{}_ps_y}(l)}{4\sigma^2_{{}_ps_x}(l)\sigma^2_{{}_ps_y}(l)}d^2\right\} \times I_0\left(\frac{\sigma^2_{{}_ps_x}(l)-\sigma^2_{{}_ps_y}(l)}{4\sigma^2_{{}_ps_x}(l)\sigma^2_{{}_ps_y}(l)}d^2\right) \tag{24}$$

which has been reported, e.g., in [37]–[39].

D. Overall Travelling Length

The overall travelling length ${}_pD$ can be obtained by the sum of all incremental lengths ${}_pd(l)$, i.e., ${}_pD = \sum_{l=1}^{L} {}_pd(l)$. Even if $L \to \infty$, none of the central limit theorems (CLT) of Lindeberg-Lévy and Lyapunov can be applied, as the incremental lengths ${}_pd(l)$ are neither identically distributed, nor independently. The correlation between the components is also not low enough to be neglected. However, the case $p = 0$ results in identically distributed incremental lengths ${}_0d(l)$ (see Section IV-C). For such a special case, the CLT for correlated random variables [40] can be invoked. To provide a closed-form solution for the overall travelling length ${}_pD$, we focus on the special case discussed in Section IV-C, where the first-order density $p_{{}_0d}(d;l) = p_{{}_0d}(d)$ follows the Rice distribution. Consequently, the CLT for correlated random variables permits us to conclude that the travelling length ${}_0D$ is a normally distributed random variable of the form $N\left(Lm_{{}_0d}, L\sigma^2_{{}_0d}\right)$, where the mean $m_{{}_0d}$ and the variance $\sigma^2_{{}_0d}$ are given by (22) and (23), respectively. This distribution can often be seen in dense and crowded areas, such as shopping centres and airports [21]–[27][5]. In Section VI, the simulation results show that for $p \geq 1$, the travelling length ${}_pD$ follows closely the log-normal distribution, which has been widely addressed in the literature [17]–[20].

V. Special Cases

As discussed in the first part of our paper, the primitive $p = 0$ allows erratic paths with sudden changes of direction. However, the higher primitives $p > 0$ result in relatively smooth paths. The level of smoothness increases by increasing p. From these two major categories, we choose $p = 0$ and $p = 1$ to further simplify some of the statistical properties of the process ${}_px(l)$. We also assume the full bridge scenario, i.e., $k_b = 1$, in the presence of a drift component, i.e., $k_d = 1$. This allows us to get a better understanding of the behaviour of ${}_px(l)$.

[5]Notice that most of the related empirical studies concern the speed distribution of mobile users, but not their travelling length. Nevertheless, the time-distance transformation allows us to extend their obtained distribution to that of the travelling length.

A. The Zeroth Primitive $p = 0$

The mean $m_{_0x}(l)$ in (6) is independent of p and remains equal to $x_s + l\delta_x$. The autocovariance function $r^c_{_0B_{x0}B_x}(l_i, l_j)$ in (5) of the standard BF simplifies to $\min(l_i, l_j)$, which complies with the result, e.g., in [31]. Subsequently, the ACF $r_{_0x_0x}(l_i, l_j)$ in (7) reduces to

$$\begin{aligned} r_{_0x_0x}(l_i, l_j) &= m_{_0x}(l_i)m_{_0x}(l_j) \\ &+ \sigma_x^2 \left(\min(l_i, l_j) - \frac{l_i l_j}{L} \right). \end{aligned} \tag{25}$$

By setting $l_i = l_j = l$ and subtracting the means' product, one can obtain the variance $\sigma^2_{_0x}(l)$ of the process $_0x(l)$ by means of the following equation

$$\sigma^2_{_0x}(l) = \sigma_x^2 l \left(1 - \frac{l}{L} \right). \tag{26}$$

The function above has a concave shape with a peak at[6] $l = L/2$ and two zeros at $l = 0$ and $l = L$. The value $\sigma^2_{_0x\max}$ of the peak then becomes $\sigma^2_{_0x\max} = \sigma^2_{_0x}(L/2) = \sigma_x^2 L/4$. Furthermore, the spatial increment $_0s_x(l)$ follows the Gaussian distribution of the form $N(\delta_x, \sigma^2_{_0s_x}(l))$, where

$$\sigma^2_{_0s_x}(l) = \sigma_x^2 \left(1 - \frac{1}{L} \right) \tag{27}$$

is the simplified version of (12) after setting $p = 0$ and $k_b = 1$. The variance $\sigma^2_{_0s_x}(l)$ in (27) can also be considered as the special case, $k_b = 1$, of its more general form in (17).

B. The First Primitive $p = 1$

In this case, the path can be attained by substituting the outcomes of the integrated (once) BF in (1). The mean $m_{_1x}(l)$ remains equal to $x_s + l\delta_x$. The auto-covariance function $r^c_{_1B_{x1}B_x}(l_i, l_j)$ in (5) of the integrated BF reduces to

$$\begin{aligned} r^c_{_1B_{x1}B_x}(l_i, l_j) &= l_i l_j \min(l_i, l_j) - \frac{l_i + l_j}{2} (\min(l_i, l_j))^2 \\ &+ \frac{1}{3} (\min(l_i, l_j))^3. \end{aligned} \tag{28}$$

For the special case of $l_i = l_j$, the auto-covariance function above becomes $l^3/3$, which agrees with the variance $\sigma^2_{_1B}(l)$ in (4) and that of reported, e.g., in [31]. The simplification of the variance $\sigma^2_{_1x}(l)$ in (9) to

$$\sigma^2_{_1x}(l) = \sigma_x^2 \frac{l^2 L}{3} \left(1 - \frac{l}{L} \right)^2 \tag{29}$$

is also very helpful to confirm its concave shape in l. The peak of the curve is again at $l = L/2$, whereas the zeros are located at $l = 0$ and $l = L$. The value $\sigma^2_{_1x\max}$ of the peak equals $\sigma^2_{_1x\max} = \sigma^2_{_1x}(L/2) = \sigma_x^2 L^3/48$. Notice that for a given value of σ_x^2 and for large values of $L \gg 1$, the maximum variance $\sigma^2_{_1x\max}$ of the process $_1x(l)$ is significantly greater than that of $_0x(l)$, i.e., $\sigma^2_{_0x\max}$ (see Section V-A). It is worth mentioning that for higher values of p, the peak is not at $L/2$ anymore. For $p \geq 2$, the position of the peak has a mild tendency to the terminating position variable, i.e., $l = L$. Furthermore, despite the apparent similarity between $\sigma^2_{_1x}(l)$ in (29) and $\sigma^2_{_0x}(l)$ in (26), a general extension to higher values of p cannot be found. For instance, the variance $\sigma^2_{_2x}(l)$ associated with the primitive $p = 2$ becomes

$$\sigma^2_{_2x}(l) = \sigma_x^2 \frac{l^2 L}{60} \left(1 - \frac{l}{L} \right)^2 (-l^2 + 6Ll + 3L^2) \tag{30}$$

which has less similarity to (26) and (29). Nevertheless, the zeros of $\sigma^2_{_2x}(l)$ in (30) are still at $l = 0$ and $l = L/2$, while its maximum occurs at the nearest natural number to $0.55L$.

VI. Numerical Results

Herein, we illustrate the statistical properties of the reference (path) model. We have also obtained these properties by means of simulation results. This means that we have generated a large enough number of realizations of the path by following the procedure described in Section V-A of Part I. Then, we have derived the statistical properties of the simulation model. An excellent match between the analytical and simulation results have been observed. Due to the similarity of the statistical properties of the reference model and the simulation model, we, nevertheless, omit to show those of the simulation model herein. In accordance with the simulation results presented in Part I of our paper, the starting point (x_s, y_s) is set to the origin of the Cartesian coordinate system, i.e., $(0\,\mathrm{m}, 0\,\mathrm{m})$, whereas the destination point (x_d, y_d), if any, is set to $(50\,\mathrm{m}, 50\,\mathrm{m})$. The number of points L is 100. The maximum standard deviation $\sigma_{_px\max}$ along the x-axis is supposed to be equal to the one along the y-axis, i.e, $\sigma_{_px\max} = \sigma_{_py\max} = \sigma_{\max}$. The only exception is where we plot the ACF $r_{_px_px}(l_i, l_j)$ of the path $_0\mathcal{T}$, which will be discussed later. Owing to space restrictions, we focus only on a special case in which the bridge to the destination point is fully established, i.e., $k_b = 1$, and the drift component is available, i.e., $k_d = 1$. The values of the primitive p is displayed in the figures and/or their captions.

Figs. 1–3 depict the ACF $r_{_px_px}(l_i, l_j)$ of $_px(l)$ in (7) for different values of the primitive p. To show the effect of the primitive p on $r_{_px_px}(l_i, l_j)$, we have used the same standard deviation $\sigma_x = \sigma_y = 2\,\mathrm{m}$ to plot the three figures. This results in completely different maximum standard deviations $\sigma_{_px\max}$ of the process $_px(l)$ (see Section V-B). The first common observation in the three figures is that the ACF $r_{_px_px}(l_i, l_j)$ varies in position index l, which indicates that the process $_px(l)$ is non-stationary. The second one is that $r_{_px_px}(l_i, 0) = r_{_px_px}(0, l_j) = 0$, which agrees with the discussion provided in Section III-C. The third observation is that the three figures are symmetric with respect to the line represented by $l_i = l_j$. Fig. 1 shows that the maximum correlation occurs at $l_i = l_j = L$, i.e., at the terminating point. This can be attributed to the fact that most of the contribution to the correlation between the samples of $_0x(l)$ is given by its drift component. As a result, the highest value of the curve occurs at $l_i = l_j = L$, where the mean value of the samples is maximum. Notice that the correlation between the random components of $_0x(l)$ is relatively low, as the non-overlapping increments of the standard BF are independent (see Section

[6]The nearest natural number to $L/2$ is acceptable as the position index l of the peak.

III of Part I). As opposed to this, integrating over the standard BF ($p > 0$) adds greatly to the correlation between the random components of ${}_0x(l)$. In this case, the contribution of the drift component to the correlation between the samples of ${}_0x(l)$ is in minority. This can be observed in Figs. 2 and 3, in which the maximum correlation occurs at (about) $l_i = l_j = L/2$, where the variance $\sigma^2_{{}_px}(l)$ is also maximum (see Section V-B).

The variance $\sigma^2_{{}_px}(l)$ of the process ${}_px(l)$ in (9) is demonstrated in Figs. 4 and 5. In accordance with Figs. 1–3, we remain on the assumption of $\sigma_x = \sigma_y = 2\,\text{m}$. Fig. 4 shows the variance $\sigma^2_{{}_px}(l)$ for different values of p. As discussed in Section III-D, $\sigma_{{}_px\,\max}$ is a monotonically increasing function in p. The significant increase in $\sigma_{{}_px\,\max}$ is the result of integrating over the BF. Referring to Fig. 4, for p equals 0 and 1, the maximum variance $\sigma_{{}_px\,\max}$ occurs at $l = 50$. For $p = 2$, the peak position, however, moves to $l = 55$, which verifies the mild tendency of the peak position to the terminating point (see Section V-B). Fig. 5 illustrates the variance $\sigma^2_{{}_2x}(l)$ in (9) for different values of the bridge parameter k_b. Herein, we have set the maximum standard deviation to $\sigma_{\max} = \sigma_{{}_2x\,\max} = 10\,\text{m}$. The importance of the figure is to show the position of the maximum variance. If $k_b = 1$, the variance $\sigma^2_{{}_2x}(l)$ is a concave function given by (30) with a peak at $l = 50$. For $k_b = 0$, the variance $\sigma^2_{{}_2x}(l)$ in (9) turns to $\sigma^2_{{}_2x}(l) = \sigma_x^2 l^5/20$, which is a monotonically increasing function in l. Therefore, the maximum occurs at $l = 100$. Finally, if $0 < k_b < 1$, the variance $\sigma^2_{{}_2x}(l)$ is a combination of a concave and convex function as shown in Fig. 5. The combined form of $\sigma^2_{{}_2x}(l)$ in the recent case can describe the special configuration of the path shown in Fig. 11 of Part I, where the trajectory first turns (as a result of the concave part of $\sigma^2_{{}_2x}(l)$) around the starting point and then leaves (as a result of the increasing tail of $\sigma^2_{{}_2x}(l)$) the close vicinity of the starting point. Notice that the curves shown in Fig. 5 show the variances of the paths along the x-axis shown in Figs. 3, 10, and 11 of Part I.

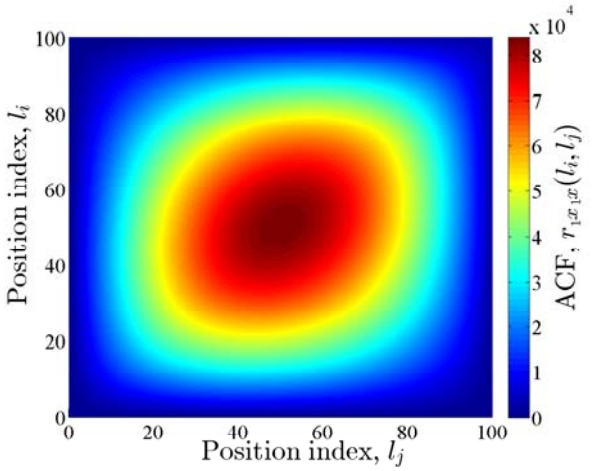

Fig. 2. The ACF $r_{{}_1x{}_1x}(l_i, l_j)$ in (7). The model parameters are $k_d = 1$, $k_b = 1$, and $\sigma_x = \sigma_y = 2\,\text{m}$.

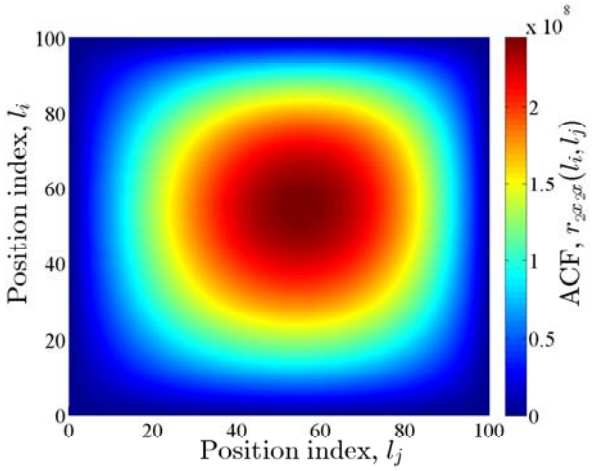

Fig. 3. The ACF $r_{{}_2x{}_2x}(l_i, l_j)$ in (7). The model parameters are $k_d = 1$, $k_b = 1$, and $\sigma_x = \sigma_y = 2\,\text{m}$.

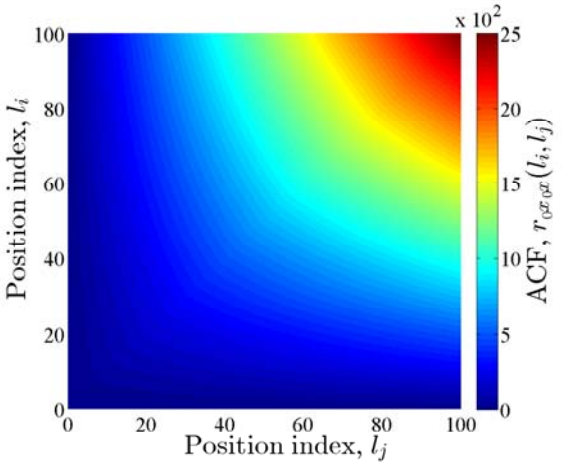

Fig. 1. The ACF $r_{{}_0x{}_0x}(l_i, l_j)$ in (7). The model parameters are $k_d = 1$, $k_b = 1$, and $\sigma_x = \sigma_y = 2\,\text{m}$.

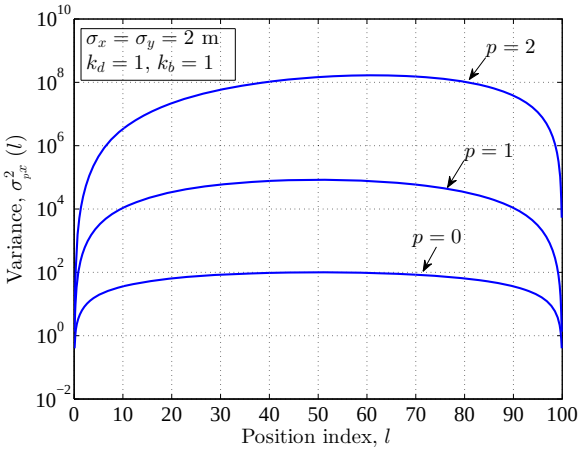

Fig. 4. The variance $\sigma^2_{{}_px}(l)$ in (9). The model parameters are $k_d = 1$, $k_b = 1$, and $\sigma_x = \sigma_y = 2\,\text{m}$.

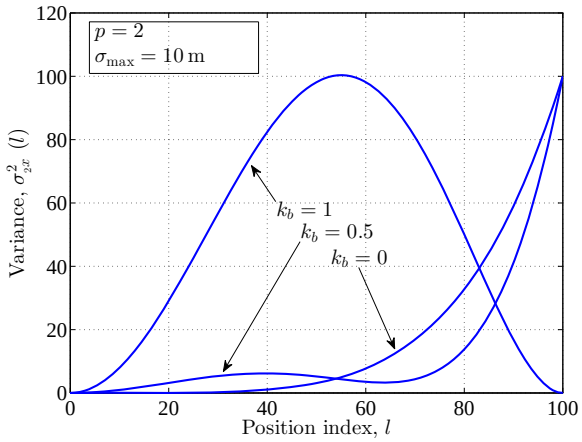

Fig. 5. The variance $\sigma^2_{2^x}(l)$ in (9). The model parameters are $k_d = 1$, $p = 2$ and $\sigma_{\max} = 10\,\mathrm{m}$.

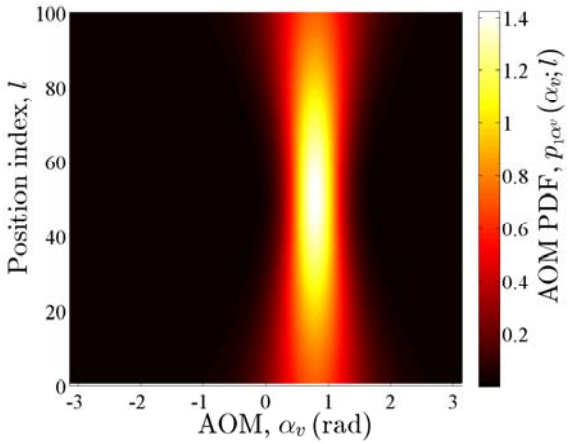

Fig. 7. The AOM PDF $p_{1^{\alpha^v}}(\alpha^v; l)$ in (14). The model parameters are $k_d = 1$, $k_b = 1$, and $\sigma_{\max} = 10\,\mathrm{m}$.

Figs. 6–8 display the AOM PDF $p_{_p\alpha^v}(\alpha^v; l)$ in (14) for different values of p. The maximum standard deviation $\sigma_{\max}$ has been set to 10 m along both axes. These figures show the AOM PDFs of the paths shown in Figs. 1–3 of Part I. As can be observed in Fig. 6, the AOM PDF $p_{_0\alpha^v}(\alpha^v; l)$ does not vary in position (look at the similarity of the colours along any given value of α^v), which indicates that the AOM process ${}_0\alpha^v$ is stationary in this case (see Section IV-B). The stationarity, however, does not hold for $p = 1$ and $p = 2$, as $p_{_p\alpha^v}(\alpha^v; l)$ changes in l (see Figs. 7 and 8). A common observation in Figs. 6–8 is that for a given l, the peak of $p_{_p\alpha^v}(\alpha^v; l)$ is at $\alpha^v = \arctan(1) = 0.78\,\mathrm{rad}$, which agrees with the slope of the drift shown in Figs. 1–3 of Part I. Moreover, by increasing p, the variance of the AOM process decreases, which is in line with the observations in Figs. 1–3 of Part I. Furthermore, for $\alpha^v = 0.78\,\mathrm{rad}$, the maximum of $p_{_p\alpha^v}(\alpha^v; l)$ occurs at $l = 50$ and $l = 55$ if $p = 1$ and $p = 2$, respectively. Finally, as opposed to many proposed mobility models in the literature, herein, the AOM is in general not uniformly distributed, which complies with real-world user tracings reported in [17].

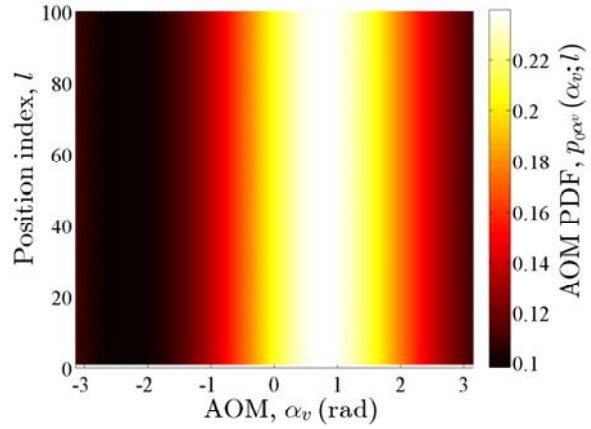

Fig. 6. The AOM PDF $p_{_0\alpha^v}(\alpha^v; l)$ in (14). The model parameters are $k_d = 1$, $k_b = 1$, and $\sigma_{\max} = 10\,\mathrm{m}$.

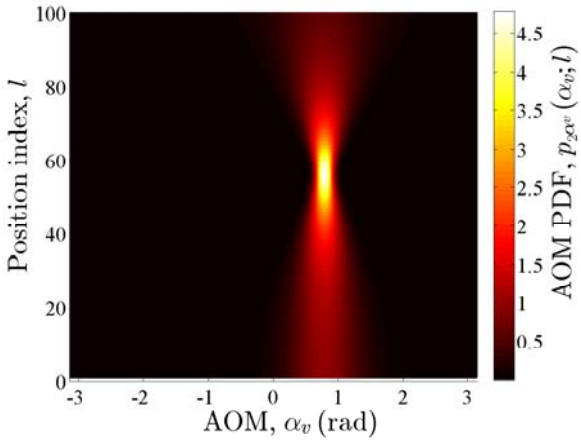

Fig. 8. The AOM PDF $p_{_2\alpha^v}(\alpha^v; l)$ in (14). The model parameters are $k_d = 1$, $k_b = 1$, and $\sigma_{\max} = 10\,\mathrm{m}$.

Figs. 9 and 10 exhibit the incremental travelling length PDF $p_{_pd}(d; l)$ in (19) for p equals 1 and 2, respectively. The model parameters are $k_d = 1$, $k_b = 1$, and $\sigma_{\max} = 10\,\mathrm{m}$. The case $p = 0$ simplifies $p_{_pd}(d; l)$ in (19) to the Rice distribution (see Section IV-D), which is trivial to be presented here. It is noteworthy that Figs. 9 and 10 show the incremental travelling length PDF $p_{_1d}(d; l)$ of the paths shown in Figs. 2 and 3 of Part I, respectively. As can be observed from both Figs. 9 and 10, $\lim_{d\to\infty} p_{_pd(l)}(d; l) = 0$, which is in agreement with the discussion in Section IV-C. Indeed, as a prerequisite for a realistic path, the proposed path model does not allow far jumps from (x_{l-1}, y_{l-1}) to (x_l, y_l). Furthermore, the variance of the incremental travelling lengths ${}_pd$ decreases by increasing the primitive p, which can also be confirmed by the paths shown in Figs. 2 and 3 of Part I. An important observation is that for a given l, the maximum $p_{_pd}(d; l)$ occurs slightly after $d = 0.5\,\mathrm{m}$. This value can be compared with the contribution of the drift component to (1), which equals $(x_d - x_s)/L = 0.5\,\mathrm{m}$. Adding the contribution of the random component in (1) to this value, the recent observation in Figs. 9 and 10 can be verified. Eventually, the variations of $p_{_pd}(d; l)$ in

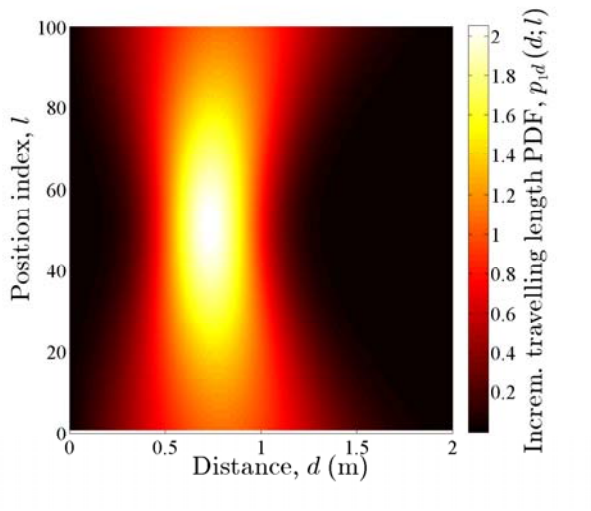

Fig. 9. The incremental travelling length PDF $p_{1d}(d;l)$ in (19). The model parameters are $k_d = 1$, $k_b = 1$, and $\sigma_{\max} = 10\,\text{m}$.

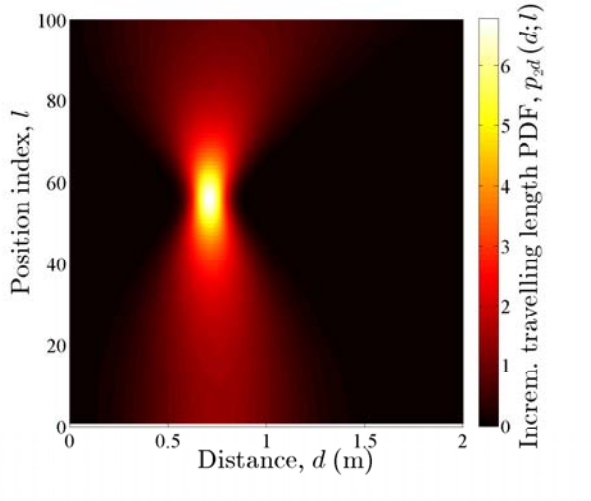

Fig. 10. The incremental travelling length PDF $p_{2d}(d;l)$ in (19). The model parameters are $k_d = 1$, $k_b = 1$, and $\sigma_{\max} = 10\,\text{m}$.

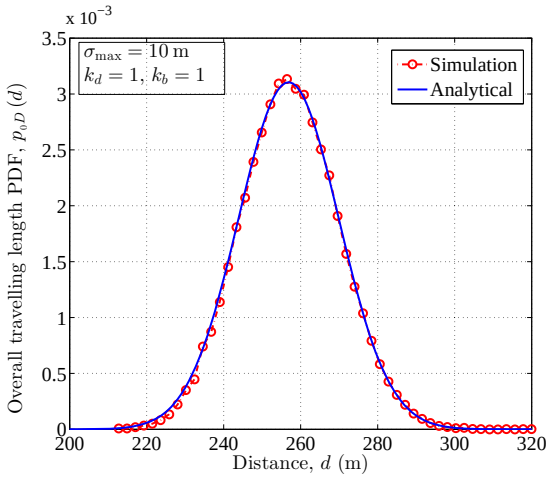

Fig. 11. The overall travelling length PDF $p_{0D}(d)$ discussed in Section IV-D. The model parameters are $k_d = 1$, $k_b = 1$, and $\sigma_{\max} = 10\,\text{m}$.

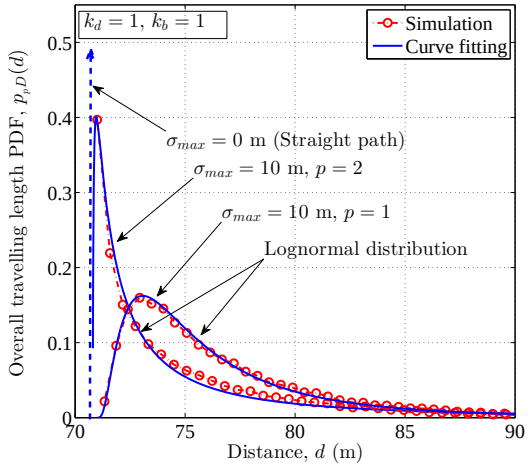

Fig. 12. The overall travelling length PDF $p_{pD}(d)$ discussed in Section IV-D. The model parameters are $k_d = 1$, $k_b = 1$, and $\sigma_{\max} = 10\,\text{m}$.

l indicate that the incremental travelling length process in (18) is non-stationary in the strict sense.

Figs. 11 and 12 demonstrate the simulated overall travelling length PDF $p_{pD}(d)$ discussed in Section IV-D. The simulation results have been obtained by computing the sum ${}_pD = \sum_{l=1}^{L} {}_pd(l)$ for 50000 realizations of the path ${}_p\mathcal{T}$ and then creating the corresponding histogram by means of 100 equally spaced bins. The model parameters are $k_d = 1$, $k_b = 1$, and $\sigma_{\max} = 10\,\text{m}$. For $p = 0$, $p_{0D}(d)$ follows the Gaussian distribution of the form $N\left(Lm_{0d}, L\sigma^2_{0d}\right)$ (see Section IV-D). In this regard, Fig. 11 shows the aforementioned Gaussian distribution, which matches excellently the simulation results. As mentioned before, the Gaussian distribution of the travelling length has been reported in empirical studies such as [21]–[27]. It is also worth mentioning that Fig. 11 represents $p_{0D}(d)$ associated with the paths shown in Fig. 1 of Part I. For $p \geq 1$, the overall travelling length PDF $p_{pD}(d)$ does not result in an analytical closed-form solution. The simulation results, however, can be obtained by the aforementioned procedure. The results shown in Fig. 12, are pertinent to the paths shown in Figs. 2 and 3 of Part I [16]. An important observation from Fig. 12 is that the travelling length PDF $p_{pD}(d)$ ($p \geq 1$) follows closely the lognormal distribution, which complies with the results from real-world tracings [17]–[20]. With reference to Fig. 12, by increasing the primitive p, both the variance and the mean of the travelling length ${}_pD$ decrease. However, the mean value cannot be less than the travelling length of the straight path. For the considered scenario, the length of the straight path equals $50\sqrt{2} = 70.7\,\text{m}$, for which the corresponding overall travelling length PDF $p_{pD}(d)$ is given by the delta Dirac function of the form $\delta(d - 70.7)$. From Fig. 12, it can be confirmed that by increasing p, the travelling length PDF $p_{pD}(d)$ tends to that of the straight path, i.e., $\delta(d - 70.7)$.

VII. Conclusion

This second part of our paper has investigated the statistical properties of the trajectory model proposed in the first part. We have studied the spatial mean, variance, and the ACF of the path model. We have also introduced a new process that is called the spatial increment process, for which we have shown that it follows the complex Gaussian distribution with nonidentical means and variances of the quadrature components. From this process, the AOM and the incremental travelling length processes of the path have been derived. We have computed the first-order density of these processes in closed form, showing that the AOM is not uniformly distributed, which agrees with real-world traces reported in the literature. We have also proved that the incremental travelling length includes the Rice and Nakagami-q distributions as special cases. Furthermore, we have computed the overall travelling length by summing up the incremental travelling lengths. Simulation results have shown that depending on the primitive order, the length of the travelling path follows either the Gaussian distribution, or the lognormal distribution, which both have been widely reported in empirical studies. To better highlight the usefulness of the model, the direct comparison of the results with empirical data is considered as a topic for future studies.

Appendix A
Derivation of the ACF $r_{{}_p x\,{}_p x}(l_i, l_j)$ in (7)

To compute $E\{{}_p x(l_i)\,{}_p x(l_j)\}$, let us recall from (1) that ${}_p x(l_i) = m_{{}_p x}(l_i) + \sigma_x W_x(l_i, k_b) = m_{{}_p x}(l_i) + \sigma_x({}_p B_x(l_i) - \frac{k_b l_i}{L}{}_p B_x(L))$, where we have replaced $x_s + k_d l_i \delta_x$ by the mean $m_{{}_p x}(l_i)$ (see (6)). This allows us to compute the ACF $r_{{}_p x\,{}_p x}(l_i, l_j)$ as follows

$$
\begin{aligned}
r_{{}_p x\,{}_p x}(l_i, l_j) &= E\{{}_p x(l_i)\,{}_p x(l_j)\} \\
&= E\left\{\left(m_{{}_p x}(l_i) + \sigma_x\left({}_p B_x(l_i) - \frac{k_b l_i}{L}{}_p B_x(L)\right)\right)\right. \\
&\quad \left.\times\left(m_{{}_p x}(l_j) + \sigma_x\left({}_p B_x(l_j) - \frac{k_b l_j}{L}{}_p B_x(L)\right)\right)\right\} \\
&= E\{m_{{}_p x}(l_i) m_{{}_p x}(l_j) \\
&\quad + \sigma_x m_{{}_p x}(l_i)\left({}_p B_x(l_j) - \frac{k_b l_j}{L}{}_p B_x(L)\right) \\
&\quad + \sigma_x m_{{}_p x}(l_j)\left({}_p B_x(l_i) - \frac{k_b l_i}{L}{}_p B_x(L)\right) \\
&\quad + \sigma_x^2\left({}_p B_x(l_i) - \frac{k_b l_i}{L}{}_p B_x(L)\right) \\
&\quad \times \left({}_p B_x(l_j) - \frac{k_b l_j}{L}{}_p B_x(L)\right)\Big\} \\
&= m_{{}_p x}(l_i) m_{{}_p x}(l_j) \\
&\quad + \sigma_x m_{{}_p x}(l_i) E\left\{{}_p B_x(l_j) - \frac{k_b l_j}{L}{}_p B_x(L)\right\} \\
&\quad + \sigma_x m_{{}_p x}(l_j) E\left\{{}_p B_x(l_i) - \frac{k_b l_i}{L}{}_p B_x(L)\right\} \\
&\quad + \sigma_x^2 E\left\{\left({}_p B_x(l_i) - \frac{k_b l_i}{L}{}_p B_x(L)\right)\right. \\
&\quad \left.\times \left({}_p B_x(l_j) - \frac{k_b l_j}{L}{}_p B_x(L)\right)\right\} \\
&= m_{{}_p x}(l_i) m_{{}_p x}(l_j) \\
&\quad + \sigma_x^2 E\left\{\left({}_p B_x(l_i) - \frac{k_b l_i}{L}{}_p B_x(L)\right)\right. \\
&\quad \left.\times \left({}_p B_x(l_j) - \frac{k_b l_j}{L}{}_p B_x(L)\right)\right\} \\
&= m_{{}_p x}(l_i) m_{{}_p x}(l_j) + \sigma_x^2\left(E\{{}_p B_x(l_i)\,{}_p B_x(l_j)\}\right. \\
&\quad - \frac{k_b l_j}{L} E\{{}_p B_x(l_i)\,{}_p B_x(L)\} \\
&\quad - \frac{k_b l_i}{L} E\{{}_p B_x(L)\,{}_p B_x(l_j)\} \\
&\quad \left. + \frac{k_b^2 l_i l_j}{L^2} E\{B_x^2(L)\}\right). \qquad (31)
\end{aligned}
$$

Finally, using $r^c_{{}_p B_x\,{}_p B_x}(\cdot,\cdot) = E\{{}_p B_x(\cdot)\,{}_p B_x(\cdot)\}$ gives the result in (7).

Appendix B
Proof of Theorem 1

With reference to the path ${}_p\mathcal{T}$ in (1), the increment process ${}_p s_x(l) = {}_p x(l) - {}_p x(l-1)$ along the x-axis can be written as

$$
\begin{aligned}
{}_p s_x(l) &= x_s + k_d l \delta_x + \sigma_x({}_p B_x(l) - \frac{k_b l}{L}{}_p B_x(L)) \\
&\quad - x_s - k_d(l-1)\delta_x - \sigma_x({}_p B_x(l-1) + \frac{k_b(l-1)}{L}{}_p B_x(L)) \\
&= k_d \delta_x + \sigma_x({}_p B_x(l) - {}_p B_x(l-1) - \frac{k_b}{L}{}_p B_x(L)). \qquad (32)
\end{aligned}
$$

The equation above represents a linear combination of zero-mean Gaussian processes plus the constant shift $k_d \delta_x$. Accordingly, the increment process ${}_p s_x(l)$ follows the Gaussian

distribution of the form $N\left(k_d\delta_x, \sigma^2_{{}_ps_x}(l)\right)$, where

$$\begin{aligned}\sigma^2_{{}_ps_x}(l) &= E\left\{(\sigma_x)^2\left({}_pB_x(l) - {}_pB_x(l-1) - \frac{k_b}{L}{}_pB_x(L)\right)^2\right\}\\ &= \sigma_x^2\, E\left\{{}_pB_x^2(l) + {}_pB_x^2(l-1) + \frac{k_b^2}{L^2}{}_pB_x^2(L)\right.\\ &- 2\,{}_pB_x(l)\,{}_pB_x(l-1) - \frac{2k_b}{L}\,{}_pB_x(l)\,{}_pB_x(L)\\ &+ \left.\frac{2k_b}{L}\,{}_pB_x(l-1)\,{}_pB_x(L)\right\}\\ &= \sigma_x^2\left(r^c_{{}_pB_x\,{}_pB_x}(l,l) + r^c_{{}_pB_x\,{}_pB_x}(l-1,l-1)\right.\\ &+ \frac{k_b^2}{L^2}r^c_{{}_pB_x\,{}_pB_x}(L,L) - 2r^c_{{}_pB_x\,{}_pB_x}(l,l-1)\\ &- \left.\frac{2k_b}{L}r^c_{{}_pB_x\,{}_pB_x}(l,L) + \frac{2k_b}{L}r^c_{{}_pB_x\,{}_pB_x}(l-1,L)\right). \quad (33)\end{aligned}$$

With the same token, the increment process ${}_ps_y(l) = {}_py(l) - {}_py(l-1)$ along the y-axis follows the Gaussian distribution of the form $N\left(k_d\delta_y, \sigma^2_{{}_ps_y}(l)\right)$, where $\sigma^2_{{}_ps_y}(l)$ is obtained from (33) by replacing the superscript x by y. Furthermore, the correlation between the increment processes ${}_ps_x(l)$ and ${}_ps_y(l)$ is zero, as their structural elements ${}_pB_x(l)$ and ${}_pB_y(l)$ are statistically independent. Therefore, the spatial increment process ${}_ps(l) = {}_ps_x(l) + j\,{}_ps_y(l)$ follows the complex Gaussian distribution of the form provided in Theorem 1.

REFERENCES

[1] T. Camp, J. Boleng, and V. Davies, "A survey of mobility models for ad hoc network research," *Wireless Communications and Mobile Computing*, vol. 2, no. 5, pp. 483–502, Sept. 2002.

[2] F. Bai and A. Helmy, *Book chapter in Wireless Ad Hoc and Sensor Networks*, Kluwer academic Publishers, 2004.

[3] J. Härri, F. Filali, and C. Bonnet, "Mobility models for vehicular ad hoc networks: a survey and taxonomy," *Communications Surveys Tutorials, IEEE*, vol. 11, no. 4, pp. 19–41, 2009.

[4] A. Einstein, "Über die von der molekularkinetischen Theorie der Wärme geforderte Bewegung von in ruhenden Flüssigkeiten suspendierten Teilchen," *Annalen der Physik*, , no. 17, pp. 549–560, May 1905.

[5] K. Pearson, "The problem of the random walk," *Nature*, vol. 72, no. 1865, pp. 294, 1905.

[6] D. B. Johnson and D. A. Maltz, *Dynamic Source Routing in Ad Hoc Wireless Networks*, vol. 353, The Kluwer International Series in Engineering and Computer Science, 1996.

[7] B. Liang and Z. J. Haas, "Predictive distance-based mobility management for PCS networks," in *Proc. 18th Annual Joint Conference of the IEEE Computer and Communications Societies (INFOCOM'99)*, 1999, vol. 3, pp. 1377–1384.

[8] V. Davis, "Evaluating mobility models within an ad hoc network," in *MS thesis, Colorado School of Mines*, 2000.

[9] M. Sánchez and P. Manzoni, "ANEJOS: a Java based simulator for ad hoc networks," *Future Generation Computer Systems*, vol. 17, no. 5, pp. 573 – 583, 2001.

[10] C. Bettstetter, G. Resta, and P. Santi, "The node distribution of the random waypoint mobility model for wireless ad hoc networks," *Mobile Computing, IEEE Transactions on*, vol. 2, no. 3, pp. 257–269, July 2003.

[11] W. Navidi and T. Camp, "Stationary distributions for the random waypoint mobility model," *Mobile Computing, IEEE Transactions on*, vol. 3, no. 1, pp. 99–108, Jan 2004.

[12] E. Hyytia, P. Lassila, and J. Virtamo, "Spatial node distribution of the random waypoint mobility model with applications," *Mobile Computing, IEEE Transactions on*, vol. 5, no. 6, pp. 680–694, June 2006.

[13] M. S. Hossain and M. Atiquzzaman, "Stochastic properties and application of city section mobility model," in *Global Telecommunications Conference, 2009. GLOBECOM 2009. IEEE*, 2009, pp. 1–6.

[14] S. Bandyopadhyay, E.J. Coyle, and T. Falck, "Stochastic properties of mobility models in mobile ad hoc networks," *Mobile Computing, IEEE Transactions on*, vol. 6, no. 11, pp. 1218–1229, 2007.

[15] J. Yoon, M. Liu, and B. Noble, "Sound mobility models," in *Proceedings of the 9th Annual International Conference on Mobile Computing and Networking*, 2003, MobiCom '03, pp. 205–216.

[16] A. Borhani and M. Pätzold, "A highly flexible trajectory model based on the primitives of Brownian fields–Part I: Fundamental principles and implementation aspects," *IEEE Trans. Wireless Commun.*, vol. 14, no. 2, pp. 770–780, Feb 2015.

[17] M. Kim, D. Kotz, and S. Kim, "Extracting a mobility model from real user traces," in *Proc. 25th IEEE International Conference on Computer Communications (INFOCOM'06)*, 2006, pp. 1–13.

[18] B. C. Csáji, A. Browet, V. A. Traag, J. Delvenne, E. Huens, P. V. Dooren, Z. Smoreda, and V. D. Blondel, "Exploring the mobility of mobile phone users," *Physica A: Statistical Mechanics and its Applications*, vol. 392, no. 6, pp. 1459 – 1473, 2013.

[19] T. Garske, H. Yu, Z. Peng, M. Ye, H. Zhou, X. Cheng, J. Wu, and N. Ferguson, "Travel patterns in China," *PLOS ONE*, vol. 6, no. 2, pp. 1–9, Feb. 2011.

[20] M. A. P. Taylor and Susilawati, "Modelling travel time reliability with the Burr distribution," *Procedia - Social and Behavioral Sciences*, vol. 54, pp. 75–83, 2012.

[21] S. B. Young, "Evaluation of pedestrian walking speeds in airport terminals," *Journal of the Transportation Research Board*, vol. 1674, no. 2, pp. 20–26, 1999.

[22] P. P. Dey, S. Chandra, and S. Gangopadhaya, "Speed distribution curves under mixed traffic conditions," *Journal of Transportation Engineering*, vol. 132, no. 6, pp. 475–481, June 2006.

[23] T. Hastie, R. Tibshirani, and J. Friedman, *The Elements of Statistical Learning: Data Mining, Inference, and Prediction*, Springer, 2001.

[24] J. Jun, "Understanding the variability of speed distributions under mixed traffic conditions caused by holiday traffic," *Transportation Research Part C: Emerging Technologies*, vol. 18, no. 4, pp. 599–610, June 2010.

[25] C.-M Hsu and F.-L Lian, "A case study on highway flow model using 2-D Gaussian mixture modeling," in *Proc. Intelligent Transportation Systems Conference, ITSC07*. Sept. 2007, pp. 790–794, Seattle, WA, USA.

[26] N. Ueda, R. Nakano, Z. Ghahramani, and G. E Hinton, "SMEM algorithm for mixture models," *Neural Computation*, vol. 12, no. 9, pp. 2109–2128, Sept. 2000.

[27] W. Zhu, K. Boriboonsomsin, and M. Barth, "Microscopic traffic flow quality of service from the drivers point of view," in *Proc. Intelligent Transportation Systems Conference, ITSC'07*. Sept. 2007, pp. 47–52, Seattle, WA, USA.

[28] A. Borhani and M. Pätzold, "Modelling of non-stationary mobile radio channels using two-dimensional Brownian motion processes," in *Proc. 6th International Conference on Advanced Technologies for Communications, ATC'13*. Oct. 2013, Ho Chi Minh City, Vietnam.

[29] A. Borhani and M. Pätzold, "Modelling of non-stationary mobile radio channels incorporating the Brownian mobility model with drift," in *Proc. World Congress on Engineering and Computer Science, WCECS13*. Oct. 2013, San Francisco, USA.

[30] A. Papoulis, *Probability, Random Variables, and Stochastic Processes*, New York: McGraw-Hill, 3rd edition, 1991.

[31] L. A. Shepp, "Radon-Nikodym derivatives of Gaussian measures," *The Annals of Mathematical Statistics*, vol. 37, no. 2, pp. 321–354, Dec. 1966.

[32] B. X. Chen and W. V. Li, "Quadratic functionals and small ball probabilities for the m-fold integrated Brownian motion," *The Annals of Probability*, vol. 31, no. 2, pp. 1052–1077, 2003.

[33] I. S. Gradshteyn and I. M. Ryshik, *Table of Integrals, Series, and Products*, Elsevier Academic Press, 7th edition, 2007.

[34] V. A. Aalo, G. P. Efthymoglou, and C. Chayawan, "On the envelope and phase distributions for correlated Gaussian quadratures," *IEEE Communications Letters*, vol. 11, no. 12, pp. 985–987, 2007.

[35] P. Dharmawansa, N. Rajatheva, and C. Tellambura, "Envelope and phase distribution of two correlated Gaussian variables," *IEEE Transactions on Communications*, vol. 57, no. 4, pp. 915–921, 2009.

[36] G. N. Watson, *A Treatise on the Theory of Bessel Functions*, Cambridge Univ. Press, 1944.

[37] M. Pätzold, *Mobile Radio Channels*, Chichester: John Wiley & Sons, 2nd edition, 2011.

[38] R. S. Hoyt, "Probability functions for the modulus and angle of the normal complex variate," *Bell Syst. Tech. J.*, vol. 26, no. 4, pp. 318–359, 1947.

[39] N. Youssef, Cheng-Xiang Wang, and M. Patzold, "A study on the second order statistics of Nakagami-Hoyt mobile fading channels," *Vehicular Technology, IEEE Transactions on*, vol. 54, no. 4, pp. 1259–1265, 2005.
[40] H. J. Hilhorst, "Central limit theorems for correlated variables: some critical remarks," *Brazilian Journal of Physics*, vol. 39, no. 2A, pp. 371–379, 2009.